# Helium-vacancy interaction in tungsten

M. S. Abd El Keriem,* D. P. van der Werf, and F. Pleiter
*Nuclear Solid State Physics, Materials Science Centre, University of Groningen, Groningen, The Netherlands*
(Received 3 September 1992; revised manuscript received 17 February 1993)

The helium-decorated In-vacancy complex $InV_2He_n$ in tungsten was studied with the aid of the perturbed-angular-correlation technique, using $^{111}In$ as a probe. The release steps $InV_2He_n \rightarrow InV_2He_{n-1}+He$ were identified for $n=1-5$. The corresponding dissociation energies are in the range of 2.9–4.5 eV, and agree perfectly well with the values determined by means of thermal-helium-desorption spectrometry. The quadrupole frequency is about 122 Mrad/s for $n=1,2$ and about 101 Mrad/s for $n=3,4$ as compared to 133 Mrad/s for the undecorated In-vacancy complex ($n=0$). Trap mutation occurs when the vacancy is filled to an occupation number $n \cong 10$, and gives rise to a quadrupole frequency of 218 Mrad/s. Trap mutation ultimately leads to bubble formation. At least three different bubble-associated quadrupole interactions were observed.

## I. INTRODUCTION

Due to their high heat of solution, inert-gas atoms are essentially insoluble in most solids. This leads to gas-atom precipitation, bubble formation, and eventually to a complete destruction of the material. Because of its obvious impact on the technology of nuclear materials, the behavior of inert gases in metals has been studied from technological considerations as well as from a more fundamental point of view, by applying a large variety of theoretical and experimental methods. A number of workshops have been held in this topic area.[1–3] From the published work, the following picture emerges.

Helium atoms in a metal may occupy either substitutional or interstitial lattice sites. As interstitials, they are very mobile at room temperature, but they will be trapped at lattice vacancies, impurities, and vacancy-impurity complexes. The potential energy of a helium atom in a metal lattice is indicated schematically in Fig. 1. In order to introduce a helium atom into the lattice, a rather large formation energy $E^f_{He}$ is required because of the closed electron shell of the helium atom from which the metal conduction band must be shielded off. For the release of a substitutional helium atom[5] from a vacancy, $V\text{He} \rightarrow V+\text{He}$, an energy $E^{diss}_{HeV}=E^b_{HeV}+E^m_{He}$ must be provided. Here, $E^b_{HeV}$ is the helium-vacancy binding energy and $E^m_{He}$ is the activation energy for interstitial helium migration. Calculated values[6] of the above-mentioned energies for tungsten are given in Table I.

Much experimental information about the behavior of helium in metals has been obtained by means of thermal-helium-desorption spectrometry (THDS). It has been applied to study helium-decorated defects in tungsten[7,8] and molybdenum.[9] After the samples had been irradiated with low-energy (0.5–1.5 keV) heavy ions, 250-eV helium atoms were injected to doses of up to about $1\times10^{14}$ at/cm$^2$. The amount of helium trapped in the crystal and the involved binding energies were determined by heating the crystal at a rate of 40 K/s. Helium desorption occurs at a number of discrete temperatures. Each release peak corresponds with a well-defined binding energy of the helium atom and flags, therefore, a particular lattice defect. From the peak contents as a function of the helium dose, the number of helium atoms per defect is obtained. The interpretation of the peaks and the corresponding desorption temperatures for tungsten are given in Table II. From these and other experimental data the following conclusions have been derived.

The next helium atom is usually less strongly bound than the previous ones. However, at a certain degree of filling the trend of smaller binding energies for higher helium filling is reversed.[11] It turns out that the volume has expanded in order to accommodate more helium atoms, i.e., the decorated monovacancy transforms into a decorated divacancy plus a self-interstitial which will be released during the subsequent annealing process:

$$V\text{He}_n+\text{He} \rightarrow V_2\text{He}_{n+1}+I \ . \quad (1)$$

This behavior has been called "trap mutation."

There are, however, a number of open questions. Some desorption peaks are weak and/or unresolved. Furthermore, $V$He and $V_2$He dissociate at approximately the same temperature (see, e.g., Ref. 9), which makes it hard

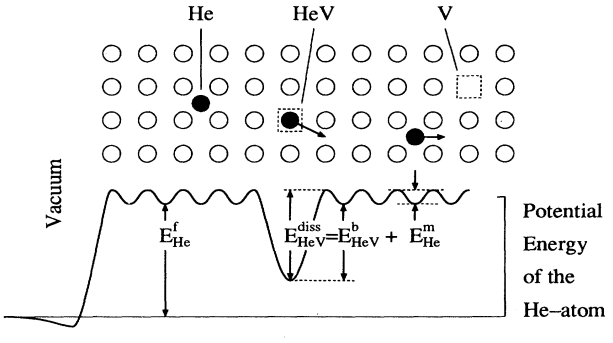


FIG. 1. Schematic view of the positions and corresponding energies of a He atom in a metal lattice (from Ref. 4).

 

TABLE I. Helium formation energy $E^f_{He}$, helium migration energy $E^m_{He}$, He-vacancy binding energy $E^b_{HeV}$, and He-vacancy dissociation energy $E^{diss}_{HeV}$, calculated for tungsten (from Ref. 6; all values in eV).

| $E^f_{He}$ | $E^m_{He}$ | $E^b_{HeV}$ | $E^{diss}_{HeV}$ |
|---|---|---|---|
| 5.47 | 0.24 | 4.15 | 4.39 |

to directly observe trap mutation in THDS. One would like to see these THDS results confirmed by an independent experiment in which a different technique is applied. We will show in this paper that the perturbed angular correlation (PAC) technique is well suited for this purpose.

## II. PERTURBED ANGULAR CORRELATION OF $\gamma$ RAYS

In this section we briefly describe some essential features of the PAC technique and its application to defect studies. For a more complete treatment we refer to the existing literature.[12–14]

Basic to the PAC method is the selection of an ensemble of excited nuclei with unequal populations of magnetic substates. As such states decay, the probability for $\gamma$-ray emission will have an anisotropic distribution with respect to the axis of quantization. In the presence of hyperfine interactions, the directional distribution becomes time dependent. In the case of polytropic interactions, the latter can be written as

$$W(\theta,t)=1+A_2G_2(t)P_2(\cos\theta)\ . \tag{2}$$

The anisotropy coefficient $A_2$ depends on the multipolarity of the emitted $\gamma$ rays. The perturbation function $G_2(t)$ contains all relevant information about the interaction of the nuclear moments with the extranuclear electromagnetic fields.

If the perturbation is due to an electric quadrupole interaction with axial symmetry, and the nuclear spin is $I=\frac{5}{2}$, we have

$$G_2(t)=\tfrac{1}{5}(1+\tfrac{13}{7}\cos\omega_0 t+\tfrac{10}{7}\cos 2\omega_0 t+\tfrac{5}{7}\cos 3\omega_0 t)\ , \tag{3}$$

where $\omega_0=(3\pi/10)eQV_{zz}/h$. Here, $Q$ is the nuclear electric quadrupole moment and $V_{zz}$ is the $z$ component of the diagonalized electric-field gradient (EFG) tensor. In defect studies, the quadrupole frequency $\omega_0$ is used to "flag" a particular defect state for identification in subsequent observations.

If the asymmetry parameter, $\eta=(V_{xx}-V_{yy})/V_{zz}$, of the EFG tensor is nonzero, the frequencies occurring in the perturbation function do, in general, not form a harmonic series. In the limiting case of $\eta=1$, there are only two different frequencies, with ratio 1:2. It is generally believed that the symmetry of the EFG tensor reflects the symmetry of the defect structure.

In the present study we used $^{111}$In as a probe. This atom, if implanted in tungsten, is known to trap vacancies. In previous PAC studies,[15–17] the In-vacancy complexes $InV_2$ and $InV_3$ have been identified (see Fig. 2), and associated with the hyperfine parameters $\omega_0=133$ Mrad/s, $\eta=0$ and $\omega_0=301$ Mrad/s, $\eta=1$, respectively. We used these clusters to monitor the He-vacancy interaction, tacitly assuming that this interaction is not significantly influenced by the presence of the $^{111}$In probe. Subsequent trapping of helium atoms, giving rise to the decorated clusters $InVHe_n$ and $InV_2He_n$, will manifest itself as a shift of the quadrupole frequency. Since the symmetry of the defects is not expected to change much upon helium decoration, trap mutation should be easily detectable in a PAC experiment through the change of the asymmetry parameter from zero to one.

It turned out that extremely small changes of the hyperfine interaction parameters were most easily recognized in the frequency domain. Therefore, fast-Fourier transformation of $G_2(t)$ became part of the standard analysis procedure.

## III. RELATION BETWEEN PAC AND THDS TEMPERATURE SCALES

Because we want to critically compare PAC and THDS results, we will discuss in this section the relation between the PAC and THDS temperature scales. In a PAC experiment, the sample is annealed during a fixed period of time, at a constant temperature. The helium desorption rate in this case is given by

$$dc(t)=-\nu_0 e^{-E/kT_{PAC}}c(t)dt\ . \tag{4}$$

We define the dissociation temperature, $T_{PAC}$, through the equation

TABLE II. Helium desorption peak assignments for helium-filled monovacancies in tungsten; $n_{He}$ is the helium occupancy before release and $T_{THDS}$ is the desorption temperature (from Ref. 10).

| Peak | $n_{He}$ | $T_{THDS}$ (K) | Assigned reaction |
|---|---|---|---|
| $H$ | 1 | 1520 | $VHe\rightarrow V+He$ |
| $G$ | 2 | 1220 | $VHe_2\rightarrow VHe+He$ |
| $F_2$ | 3 | 1130 | $VHe_3\rightarrow VHe_2+He$ |
| $F_1$ | 4 | 1080 | $VHe_4\rightarrow VHe_3+He$ |
| $E$ | 5–9 | 960 | $VHe_n\rightarrow VHe_4+(n-4)He$ |

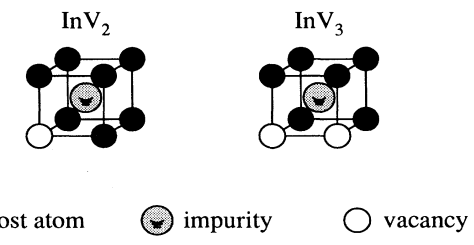


FIG. 2. Configurations of the In-vacancy complexes $InV_2$ and $InV_3$. The In atom is located close to a regular lattice site.

$$c(t_0)=c(0)\exp\{-\nu_0 t_0 e^{-E/kT_{\mathrm{PAC}}}\}=\tfrac{1}{2}c(0)\ , \tag{5}$$

i.e., the temperature at which the sample must be kept during a time $t_0$ in order to dissociate 50% of the number of defects. Substituting $\nu_0=2\times10^{14}$ Hz for the attempt frequency and $t_0=900$ s for the annealing time, we obtain ($E$ in eV, $T$ in K)

$$E=0.003\,45T_{\mathrm{PAC}}\ . \tag{6}$$

In a THDS experiment, ramp heating is applied at a typical rate of $\alpha=40$ K/s, and the number of helium-decorated defects is obtained by integrating Eq. (4):

$$c(t_0)=c(0)-\int_0^{t_0}\nu_0 e^{-E/kT(t')}c(t')dt'\ , \tag{7a}$$

$$c(T_{\mathrm{THDS}})=c(T_0)-(\nu_0/\alpha)(E/k)\times\int_{E/kT_{\mathrm{THDS}}}^{E/kT_0}(e^{-u}/u^2)c(u)du\ . \tag{7b}$$

If $T_{\mathrm{THDS}}\gg T_0$, we may replace the integral by the value of the integrand at $T_{\mathrm{THDS}}$, yielding

$$c(T_{\mathrm{THDS}})=c(T_0)/[1+(\nu_0/\alpha)(E/k)(kT_{\mathrm{THDS}}/E)^2e^{-E/kT_{\mathrm{THDS}}}]\ . \tag{8}$$

Substituting the previously mentioned values of $\nu_0$ and $\alpha$ in Eq. (8), and using our definition of the dissociation temperature, we obtain the relation ($E$ in eV, $T$ in K)

$$E=8.62\times10^{-5}T_{\mathrm{THDS}}\ln(4.1\times10^{8}T_{\mathrm{THDS}}^2/E)\ . \tag{9}$$

Figure 3 illustrates the relation between the activation energy $E$ and the dissociation temperatures $T_{\mathrm{PAC}}$ and $T_{\mathrm{THDS}}$, as calculated from Eqs. (5) and (9). In the interesting temperature region around 1000 K, we have, to good approximation,

$$T_{\mathrm{PAC}}\simeq0.82T_{\mathrm{THDS}}\ . \tag{10}$$

## IV. EXPERIMENTAL DETAILS

All samples were polycrystalline tungsten foils with a purity of 99.95%, which had been annealed in vacuum ($p\approx1\times10^{-6}$ mbar) at 1270 K for 30 min in order to remove the surface oxide layer. The work described in this paper includes two series of experiments.

In the first series, the samples were implanted with 50-keV $^{111}$In ions to a dose of less than $5\times10^{12}$ at/cm$^2$ and subsequently annealed at 750 K for about 15 min (see Sec. V). It is known that at the chosen temperature only the $InV_2$ cluster is stable, whereas the $InV_3$ cluster dissociates.[18] The standard treatment creates a defect population with about 25% of the $^{111}$In atoms located in $InV_2$ complexes. The remaining $^{111}$In atoms are either located at substitutional sites or associated with small vacancy clusters. Next, the samples were implanted with 300-eV $^4He^+$ ions to a dose of about $3\times10^{15}$ at/cm$^2$. The maximum energy transferred by the helium ions to the lattice amounts to 26 eV, which is well below the minimum displacement energy. Therefore, no further damage is introduced in the samples by these helium implantations. After this preparative treatment, the samples were annealed at stepwise increasing temperatures in the range from 800 up to about 1700 K.

Guided by the results obtained in the first series of experiments, we prepared the samples for the second series in a slightly different way. After implantation of $^{111}$In and subsequent annealing at 750 K, the samples were postimplanted with helium to a dose of $1\times10^{14}$ at/cm$^2$ and annealed at 1220 K. At this temperature, voids and all undecorated vacancies disappear from the sample while bubbles do not yet develop, and $InV_2He$ is the only visible defect in the PAC spectrum [Fig. 5(a)]. Starting from this relatively clean situation, we proceeded in two different ways. Some of the samples were implanted with additional helium atoms to a dose of $3\times10^{14}$ at/cm$^2$ and annealed at temperatures in the range from 650 up to 1320 K, in order to study the release of helium from the decorated monovacancies (see Sec. VI). Other samples, used to investigate trap mutation, were postimplanted with helium doses varying from $3\times10^{13}$ at/cm$^2$ to $9\times10^{14}$ cm$^{-2}$ (see Sec. VII). The annealing time in each series of experiments was 15 min; all PAC measurements were carried out at room temperature. The observed In-vacancy and In-vacancy-helium defects, the corresponding hyperfine interaction parameters $\omega_0$ and $\eta$, and the temperature ranges in which the defects were found to be stable are collected in Table III.

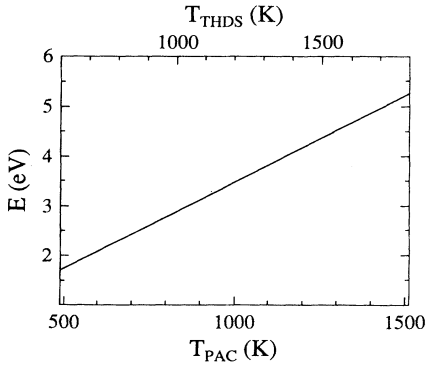


FIG. 3. Relation between the activation energy $E$ and the dissociation temperatures $T_{\mathrm{PAC}}$ and $T_{\mathrm{THDS}}$, as calculated from Eqs. (6) and (9).

## V. EXPLORATORY MEASUREMENTS

After the sample treatment for the first series of experiments, described in Sec. IV, only a single component is visible in the Fourier transform of the PAC spectrum,

TABLE III. In-vacancy and In-vacancy-helium defects observed by means of PAC, He occupancy $n_{He}$, corresponding THDS labels, hyperfine interaction parameters $\omega_0$ and $\eta$, and temperature ranges in which the defects were observed.

| Defect | $n_{He}$ | THDS label | $\omega_0$ (Mrad/s) | $\eta$ | Temperature range (K) |
|---|---|---|---|---|---|
| $InV_2$ | 0 | | 133 | 0 | 550–800 |
| $InV_2He_n$ | 1 | $H$ | 121 | 0 | 1085–1300 |
| | 2 | $G$ | 122 | 0 | 1000–1085 |
| | 3 | $F_2$ | 100 | 0 | 900–1000 |
| | 4 | $F_1$ | 102 | 0 | 835–900 |
| | 5–9 | $E$ | ? | ? | <835 |
| $InV_3$ | 0 | | 301 | 1 | 600–720 |
| $InV_3He_n$ | >9 | $I$ | 218 | 1 | 850–1300 |
| Microvoids | 0 | | 249 | 0 | 850–1050 |
| Bubbles | >50 | $J$ | 255 | 0.35 | 1400–1700 |
| | | | 275 | 0 | |
| | | | 283 | 0 | |

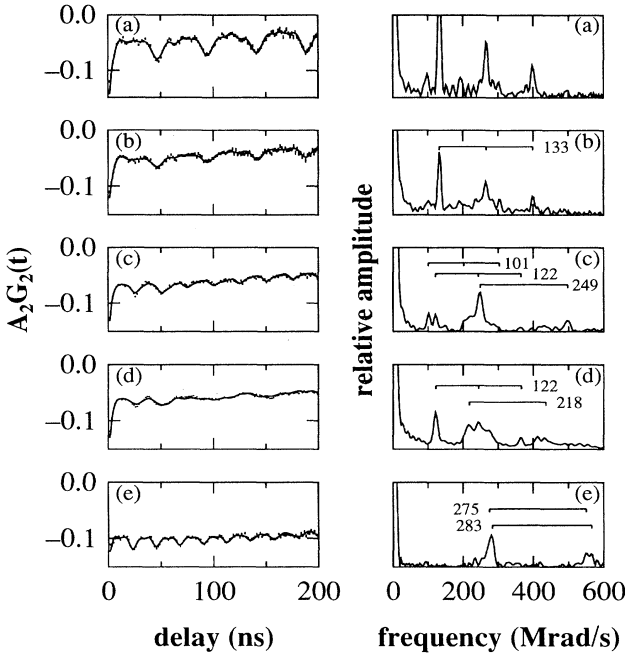


FIG. 4. PAC spectra (left) and their Fourier transforms (right) measured (a) before helium implantation, (b) after helium implantation to a dose of $3\times10^{15}$ at/cm$^2$, and subsequent annealing at (c) 920–1020 K, (d) 1050–1250 K, and (e) 1400–1600 K.

with hyperfine interaction parameters $\omega_0=133$ Mrad/s and $\eta=0$. During the subsequent helium implantation approximately 50% of the vacancies in the sample are decorated. No new precessional signals are observed: the Fourier power is apparently distributed over many frequencies because of a large range of helium occupancies. By increasing the temperature, an increasing number of helium atoms is released and the Fourier power contracts at a few well-defined frequency values. The PAC spectra and their Fourier transforms obtained before and after helium implantation, and after subsequent annealing at temperatures in the ranges 920–1020, 1050–1250, and 1400–1600 K are shown in Fig. 4. The spectra obtained in each range of temperatures were summed in order to improve statistics. The results can be summarized as follows.

In the temperature region 920–1020 K, three components are observed with quadrupole frequencies of 101, 122, and 249 Mrad/s, all with an asymmetry parameter $\eta=0$. The third frequency is known from previous work and has been assigned to microvoids.[15–17] These voids disappear at about 1000 K. The 122-Mrad/s component grows at 1030 K at the expense of the 101-Mrad/s component, and disappears at 1320 K. In the temperature region 1050–1250 K, a new component is visible, with a quadrupole frequency of about 218 Mrad/s and an asymmetry parameter varying from 0.9 to 1.0.

Considering the observed symmetry properties (cf. Table III), we tentatively conclude that the 101- and 122-Mrad/s components are related to $InV_2He_n$, while the 218-Mrad/s component has to be associated with $InV_3He_n$. Note that the undecorated clusters $InV_2$ and $InV_3$ give rise to asymmetry parameters 0 and 1, respectively.[15–17] We attribute the gradual change of $\eta$ from 0.9 to 1.0 to the release of helium atoms, one by one, from the $InV_3He_n$ cluster.

Finally, in the temperature region 1400–1600 K, we observed growth of helium bubbles. They give rise to quadrupole frequencies of 275 and 283 Mrad/s, each with an asymmetry parameter $\eta=0$, and 255 Mrad/s with an asymmetry parameter $\eta=0.35$.

## VI. ANNEALING BEHAVIOR OF HELIUM-DECORATED MONOVACANCIES

From the results obtained in the exploratory experiments (Sec. V) we learned that during annealing at 1220 K undecorated vacancies and voids disappear and helium-filled bubbles do not yet develop. Therefore, a sample treated in this way gives rise to a Fourier spectrum that contains only the 122-Mrad/s component. We postimplanted two such samples with an additional helium dose of $3\times10^{14}$ at/cm$^2$ and annealed them at stepwise increasing temperatures in the range 650–1320 K, in order to investigate the thermal stability of $InV_2He_n$ in more detail. Some typical PAC results are shown in Fig. 5.

After implantation of the additional helium, the amplitude of the 122-Mrad/s peak in the Fourier spectrum had decreased to about 30% of its original value, indicating that many helium atoms had been trapped. These atoms were successively "boiled off" during the next annealing steps, according to the reactions

$$InV_2He_n \rightarrow InV_2He_{n-1}+He\ . \tag{11}$$

At temperature $T_{PAC}=1300(25)$ K, the last helium atom is released and the remaining defect, $InV_2$, dissociates. This step corresponds with the $H$ peak observed in THDS at 1520 K (Table II). The ratio of PAC and

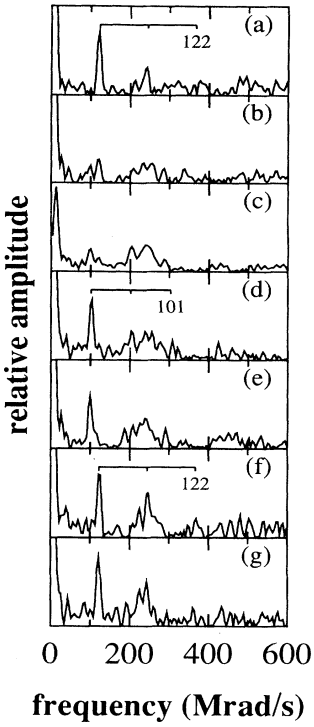


FIG. 5. Fourier spectra measured (a) after postannealing at 1220 K, (b) after additional helium implantation to a dose of $3\times10^{14}$ at/cm$^2$, and after subsequent annealing at (c) 800 K, (d) 875 K, (e) 950 K, (f) 1075 K, and (g) 1225 K.

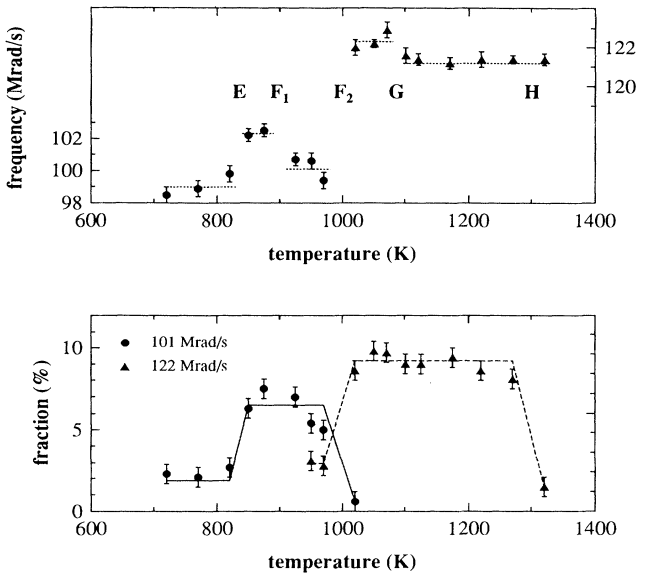


FIG. 6. Average quadrupole frequencies (top) and defect fractions (bottom), as a function of the annealing temperature.

THDS dissociation temperatures is 0.855(16), which agrees fairly well with Eq. (10).

The different helium-decorated defects give rise to frequencies that cluster in two groups, at about 101 and 122 Mrad/s. The PAC spectra were, therefore, analyzed with two components. Average quadrupole frequencies and corresponding defect fractions are plotted in Fig. 6, as a function of the annealing temperature. The quadrupole frequency changes significantly at $T_{\rm PAC}=835(15)$, 900(15), 1000(25), and 1085(15) K. These steps correspond with the $E$, $F_1$, $F_2$, and $G$ peaks, respectively, in the THDS spectrum. The asymmetry parameter is not affected by the annealing and remains zero.

Dissociation temperature, $T_{\rm PAC}$, and dissociate energy, $E$, are related through Eq. (6). The resulting energy values are given in Table IV. The quoted errors merely account for the uncertainty in the dissociation temperature. The PAC energies are in perfect agreement with the corresponding THDS values, which are also given in Table IV. The helium-vacancy binding energies are, apparently, not measurably influenced by the presence of the $^{111}$In probe.

In the temperature region 850–1270 K, the sum of the two fractions is constant within limits of error, and only slightly smaller than the initial In$V_2$He fraction of 10% measured before the additional helium had been implanted [cf. Figs. 5(a) and 5(g)]. Apparently, less than 10% of the traps have mutated.

Assuming a Poisson distribution, we may write the probability of trapping $i$ helium atoms as

$$p_i=\frac{\langle n\rangle^i}{i!}e^{-\langle n\rangle}\ . \tag{12}$$

According to the trapping cross section derived in the next section, the additional helium dose of $3\times10^{14}$ at/cm$^2$ gives rise to trapping of an average of $\langle n\rangle=7$ helium atoms. From the probability distribution defined by Eq. (12) and the fact that no components with a fraction of more than 2% are visible in the spectra measured at temperatures below 850 K, we conclude that the Fourier power is distributed over at least five different (unobserved) frequencies. We conjecture that the $E$ peak marks the release of at least five helium atoms. Therefore, a helium occupancy of $n\geq10$ is required for trap mutation to take place.

## VII. HELIUM-INDUCED TRAP MUTATION

In the exploratory measurements (Sec. V) a new frequency peak was observed at 218 Mrad/s, in the temper-

TABLE IV. He-vacancy dissociation energies for the $n_{\rm He}$th He atom, obtained by means of PAC and THDS. All values in eV.

| Peak | $n_{\rm He}$ | PAC | THDS |
|---|---|---|---|
| $H$ | 1 | 4.50(9)[a] | 4.60[b] |
| $G$ | 2 | 3.75(5)[a] | 3.69[c] |
| $F_2$ | 3 | 3.46(9)[a] | 3.42[c] |
| $F_1$ | 4 | 3.11(9)[a] | 3.27[c] |
| $E$ | 5–9 | 2.89(5)[a] | 2.91[c] |

[a]This work.
[b]Reference 7.
[c]Derived by scaling from $T_{\rm THDS}$ (see Table II).

ature region 1050–1250 K. According to the observed symmetry, we tentatively assigned this peak to the helium-filled divacancy, $InV_3He_n$. In order to obtain additional support for this interpretation, we varied the additional helium dose from $3\times10^{13}$ at/cm$^2$ up to $9\times10^{14}$ at/cm$^2$ and monitored the intensity of the 122-Mrad/s component. In Fig. 7, we plotted the result as a function of the additional helium dose. The intensities were corrected for a small, dose-independent contribution of unknown origin. An effective trapping cross section of $\mu_{\text{eff}}=2\times10^{-14}$ cm$^2$ is derived from the initial slope of the plot. The inverse of the cross section, $5\times10^{13}$ at/cm$^2$, is equal to the helium dose needed to trap, at the average, one helium atom.

The trapping cross section may be expressed as (see Ref. 18 and references cited therein)

$$\mu=\frac{z\eta\langle x\rangle}{\Gamma\lambda^2 N_0} . \tag{13}$$

Substituting an effective trapping radius $z=2$ (from Ref. 19), an implantation efficiency $\eta\cong0.6$, and average implantation depth $\langle x\rangle\cong4a$ (from a TRIM simulation), a geometry factor $\Gamma=\frac{1}{6}$, an elementary jump length $\lambda=a/2$, an atomic density $N_0=2/a^3$, and the lattice parameter $a=3.16$ Å, we obtain $\mu=6\times10^{-14}$ cm$^2$. This is only slightly larger than the experimental value, which proves that the trap density after the special sample treatment is extremely small indeed.

We further monitored the intensity of the 218-Mrad/s component as a function of the additional helium dose. In Fig. 8, we show some of the PAC spectra that were measured before implantation of additional helium, and after helium implantation and subsequent annealing at 1270 K. The annealing treatment is necessary in order to "boil off" excessive helium atoms. In the high-dose regime, the $InV_2He$ fraction does not recover to its original value because of trap mutation [compare left-hand and right-hand sides of Fig. 8(c)]. We are aware of the fact that part of the intensity at 218 Mrad/s may arise from $InV_3$ complexes that have survived the preparative annealing treatment at 750 K (Sec. IV). In Fig. 9, we plotted, therefore, the intensity increment vs the average helium occupancy calculated from the previously mentioned trapping cross section. The intensity increases to a maximum of about 25% for an average occupancy $\langle n\rangle\cong13$. We consider this to be strong evidence that trap mutation has occurred indeed. According to this interpretation, the decrease to zero of the intensity increment for $\langle n\rangle=19$ is a consequence of multiple trap mutation.

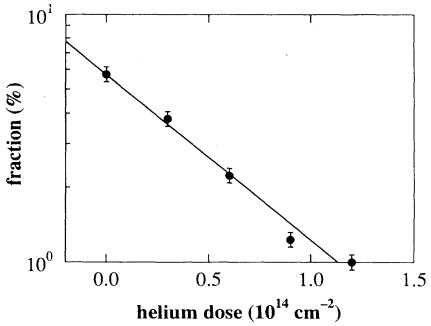


FIG. 7. Fraction of $InV_2He$ as a function of the additional helium dose.

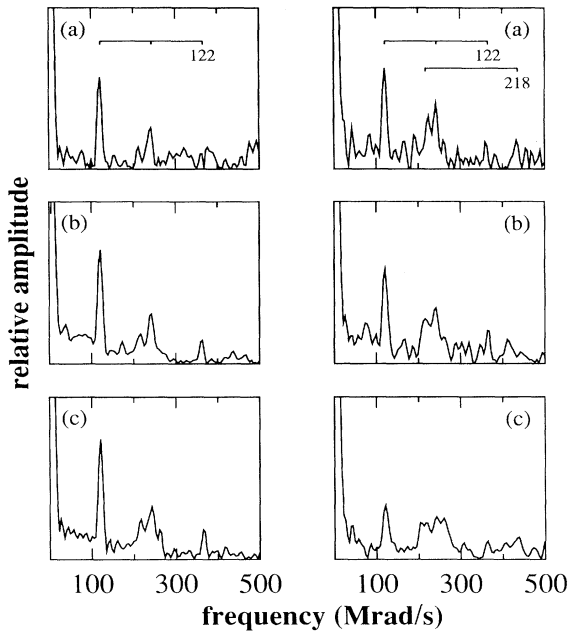


FIG. 8. Right: Fourier spectra measured after implantation of additional helium to a dose of $3\times10^{14}$ at/cm$^2$ (a), $6\times10^{14}$ at/cm$^2$ (b), and $9\times10^{14}$ at/cm$^2$ (c), and subsequent annealing at 1270 K. Left: corresponding spectra measured before the helium implantation.

The relative number of mutated traps is

$$p=\sum_{i=n_1}^{n_2=1} p_i , \tag{14}$$

where $p_i$ is given by Eq. (12). The numbers $n_1$ and $n_2$

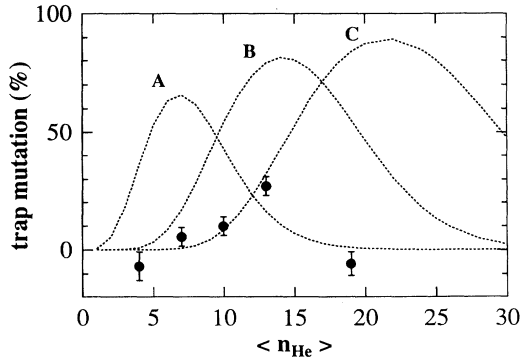


FIG. 9. Relative number of trap mutations vs average helium occupancy $\langle n_{\text{He}}\rangle$. Solid points were obtained in the present experiments. Dotted curves were calculated from Eq. (14), assuming that mutation occurs after trapping of (a) the 5th, (b) the 10th, or (c) the 15th helium atom.

denote the helium occupancies at which the trap mutates for the first and the second times, respectively. The dotted curves in Fig. 9 were calculated assuming $n_1 = n_2$. Comparing the maxima of the calculated curves and the experimental data, we conclude that $n_1 \cong 10$. This is in agreement with the conclusion arrived at in the previous section.

The discrepancy between experimental and calculated values may be caused by the depth distribution of $InV_2$ and/or by the fact that the number of helium atoms required for trap mutation decreases as the size of the vacancy cluster increases. Both effects will lead to a reduction of the number of traps that have mutated precisely once.

## VIII. CONCLUSIONS

We have investigated the complexes $InV_2He_n$ in tungsten. We were able to identify the release steps $InV_2He_n \rightarrow InV_2He_{n-1} + He$ for $n = 1-5$. The derived dissociation energies are in the range 2.9–4.5 eV, and agree perfectly well with the values determined by means of THDS. The dissociation energy seems not to be influenced by the presence of the $^{111}$In probe. The quadrupole frequency, $\omega_0$, is about 122 Mrad/s for $n = 1,2$, whereas for $n = 3,4$ the frequencies cluster at about 101 Mrad/s. In all cases, the quadrupole frequencies are smaller than that for the undecorated vacancy. Trap mutation occurs when the vacancy is filled to an occupation number $n \cong 10$, and gives rise to a quadrupole frequency of 218 Mrad/s. Trap mutation ultimately leads to bubble formation. We have observed at least three different bubble-associated quadrupole interactions.

## ACKNOWLEDGMENTS

This work was part of the research program of the Stichting voor Fundamenteel Onderzoek der Materie (FOM) and was made possible by financial support from the Nederlandse Organisatie voor Wetenschappelijk Onderzoek (NWO). One of us (M. S. Abd El Keriem) gratefully acknowledges financial support by the Egyptian Ministry of Higher Education.

---

*On leave from Ain Shams University, Cairo, Egypt.

[1] *Proceedings of the Harwell Consultants' Symposium on Rare Gases in Metals and Alkali Halides,* edited by S. F. Pugh [Radiat. Eff. **53**, 105 (1980)].

[2] *Proceedings of the Jülich Symposium on Fundamental Aspects of Helium in Metals,* edited by H. Ullmaier (Gordon and Breach, New York, 1983); see Radiat. Eff. **78**, 1 (1983).

[3] *Fundamental Aspects of Inert Gases in Solids,* edited by S. E. Donnelly and J. H. Evans (Plenum, New York, 1991).

[4] W. Schilling, in *Point Defects and Defect Interactions in Metals,* edited by J.-I. Takamura, M. Doyama, and M. Kiritani (North-Holland, Amsterdam, 1982), p. 303.

[5] We write $VHe_n$ for a lattice defect that consists of a vacant lattice site and $n$ helium atoms. In this notation, $V$He denotes a substitutional helium atom, $VHe_2$ a monovacancy occupied by two helium atoms, etc.

[6] W. D. Wilson and R. A. Johnson, in *Interatomic Potentials and Simulation of Lattice Defects,* edited by P. C. Gehlen, J. R. Beeler, and R. I. Jaffee (Plenum, New York, 1972), p. 375.

[7] A. A. Van Gorkum, J. Appl. Phys. **51**, 2594 (1980).

[8] G. J. van der Kolk, A. van Veen, L. M. Caspers, and J.Th.M. de Hosson, J. Nucl. Mater. **127**, 56 (1985).

[9] A. van Veen, J. H. Evans, W.Th.M. Buters, and L. M. Caspers, Radiat. Eff. **78**, 53 (1983).

[10] A. van Veen, Materials Sci. Forum **15-18**, 3 (1987).

[11] E. V. Kornelsen and A. A. van Gorkum, J. Nucl. Mater. **92**, 79 (1980).

[12] R. M. Steffen and K. Alder, in *The Electromagnetic Interaction in Nuclear Spectroscopy,* edited by W. D. Hamilton (North-Holland, Amsterdam, 1975), Chaps. 12 and 13.

[13] Th. Wichert and E. Recknagel, in *Microscopic Methods in Metals,* edited by U. Gonser, Topics in Current Physics Vol. 40 (Springer, Berlin, 1986), p. 317.

[14] A. R. Arends, C. Hohenemser, F. Pleiter, H. de Waard, L. Chow, and R. M. Suter, Hyperfine Interact. **8**, 1991 (1980).

[15] U. Pütz, A. Hoffmann, H. J. Rudolph, and R. Vianden, Z. Phys. B **46**, 107 (1982).

[16] K. Post, F. Pleiter, G. J. van der Kolk, A. van Veen, L. M. Caspers, and J.Th.M. de Hosson, Hyperfine Interact. **15/16**, 421 (1983).

[17] G. J. van der Kolk, K. Post, A. van Veen, F. Pleiter, and J.Th.M. de Hosson, Radiat. Eff. **84**, 131 (1985).

[18] J. R. Fransens, M. S. Abd El Keriem, and F. Pleiter, J. Phys. Condens. Matter **3**, 9871 (1991).

[19] R. H. J. Fastenau, A. van Veen, P. Penning, and L. M. Caspers, Phys. Status Solidi A **47**, 577 (1978).